

Analysis of urban atmospheric influence on free-space quantum key distribution

Hai-Long Zhang(张海龙), Xing-Ran Chen(陈星燃), and Tan Li(李坦)
Citation: Chin. Phys. B, 2026, 35 (**4**): 040306. DOI: 10.1088/1674-1056/ae0bfc
http://cpb.iphy.ac.cn; http://iopscience.iop.org/cpb

What follows is a list of articles you may be interested in

Free-space discrete-variable quantum key distribution in a mountainous environment

Xing-Ran Chen(陈星燃), Jian-Hong Shi(史建红), and Hai-Long Zhang(张海龙)
Chin. Phys. B, 2025, 34 (**5**): 050301. DOI: 10.1088/1674-1056/adbd25

Deep-learning-assisted optical communication with discretized state space of structured light

Minyang Zhang(张敏洋), Dong-Xu Chen(陈东旭), Pengxiang Ruan(阮鹏祥), Jun Liu(刘俊), Dong-Zhi Fu(付栋之), Jun-Long Zhao(赵军龙), and Chui-Ping Yang(杨垂平)
Chin. Phys. B, 2024, 33 (**12**): 120304. DOI: 10.1088/1674-1056/ad8553

Performance analysis of quantum key distribution using polarized coherent-states in free-space channel

Zengte Zheng(郑增特), Ziyang Chen(陈子扬), Luyu Huang(黄露雨),Xiangyu Wang(王翔宇), and Song Yu(喻松)
Chin. Phys. B, 2023, 32 (**3**): 030306. DOI: 10.1088/1674-1056/ac7450

Analysis of atmospheric effects on the continuous variable quantum key distribution

Tao Liu(刘涛), Shuo Zhao(赵硕), Ivan B. Djordjevic, Shuyu Liu(刘舒宇), Sijia Wang(王思佳), Tong Wu(吴彤), Bin Li(李斌), Pingping Wang(王平平), and Rongxiang Zhang(张荣香)
Chin. Phys. B, 2022, 31 (**11**): 110303. DOI: 10.1088/1674-1056/ac6b1f

Short-wave infrared continuous-variable quantum key distribution over satellite-to-submarine channels

Qingquan Peng(彭清泉), Qin Liao(廖骎), Hai Zhong(钟海), Junkai Hu(胡峻凯), and Ying Guo(郭迎)
Chin. Phys. B, 2022, 31 (**6**): 060306. DOI: 10.1088/1674-1056/ac490a

---

Analysis of urban atmospheric influence on free-space quantum key distribution

Hai-Long Zhang(张海龙)†, Xing-Ran Chen(陈星燃), and Tan Li(李坦)

Henan Key Laboratory of Quantum Information and Cryptography, SSF, IEU, Zhengzhou 450001, *China*

(Received 24 June 2025; revised manuscript received 24 September 2025; accepted manuscript online 26 September 2025)

Quantum key distribution (QKD) has been widely deployed in practical applications after decades of development. However, the QKD system is easily affected by the external environment, especially free-space QKD. In this text, we examine two scenarios of free-space QKD in urban environments: satellite to ground and intercity. For satellite to ground QKD, the effects of stray light are analyzed. For intercity link, we discuss the influence of sea salt particles in coastal cities, and insoluble and soot particles in inland cities. Our findings indicate that using a telescope with a smaller field of view (FOV) and larger aperture diameters in satellite-to-ground QKD can effectively reduce errors induced by stray light. However, the diameter cannot be increased infinitely, when exceeding 0.8 m, the number of stray photons entering receiver rises rapidly and the quantum bits error rate (QBER) shows no significant reduction. For intercity QKD, the strength of extinction varies with relative humidity and aerosol particle radius, consequently altering channel transmittance. We investigate the impact of sea salt, insoluble particles, and soot on the key rate, finding that under the number density $N = 10^6$ m^{-3}, sea salt exhibits the strongest impacts on key rate, especially when radius exceed 2.5 μm. The impacts of insoluble particles are weaker and soot is the weakest, which can be ignored until N reaches 10^9 m^{-3}. For larger particle density, we can get higher key rate and further transmission distances in a soot-dominated environment. Our work could provide a valuable reference for the practical implementation of QKD in urban atmospheres.

Keywords: free-space, aerosol particles, urban atmosphere, key rate

PACS: 03.67.Dd, 03.67.Hk, 03.67.–a

DOI: 10.1088/1674-1056/ae0bfc **CSTR:** 32038.14.CPB.ae0bfc

1. Introduction

Quantum key distribution (QKD)[1] is a technique that leverages fundamental quantum mechanical principles, such as the non-cloning theorem, to realize unconditional security, enabling two communicating parties to negotiate a legal secret key. The first QKD protocol BB84 was proposed by Bennett *et al.*[2] in 1984. After decades of development, QKD has matured into a robust tool for ensuring secure communications. The transmission channels of quantum states can be generally divided into optical fiber channel and free-space channel.[3] In comparison to the two channel types, free-space QKD has been studied intensively due to its characteristics of broader geographical coverage and more flexible system deployment compared to fiber-based systems. In quantum communication, it has been widely utilized, especially in the satellite, intercity, and other practical scenarios. However, the free-space channel exhibits significantly greater complexity compared to fiber-based systems due to fog,[4] turbulence,[5] various weather conditions in the atmosphere, and disturbances caused by human activity. Investigating the impacts of these factors on practical QKD systems is greatly essential.

Given the extensive global distribution of urban areas, the optical beam in free-space QKD inevitably interacts with urban atmospheric environments. Stray light,[6] such as street light and anthropogenic illumination, and some aerosol particles that lead to scattering, extinction, and beam wandering[7] are all key factors affecting free-space QKD. Simultaneously, successful implementation of QKD in urban areas is the key to constructing urban quantum networks, thus it is important to establish proper models to evaluate the influence of these factors on QKD systems.

For these purposes, our paper is organized as follows. In Section 2, we analyze the impact of urban stray light on free-space QKD; according to atmospheric illumination intensity across different urban areas and weather conditions, the number of stray photons per pulse received at the detector is calculated. Based on the scenario of satellite-ground link, we quantitatively evaluate the quantum bits error rate (QBER) and systematically discuss effective measures to reduce the QBER. In Section 3, the effects of aerosol particles in urban areas are studied for intercity QKD links. According to the different locations of cities, we analyze three types of aerosol particles, including their extinction effects and influence on atmosphere transmittance. We also compare the extinction strengths of the three aerosol types. In Section 4, key rate analysis is given. The conclusions are drawn in Section 5.

†Corresponding author. E-mail: zhhl049@126.com

© 2026 Chinese Physical Society and IOP Publishing Ltd. All rights, including for text and data mining, AI training, and similar technologies, are reserved.

2. Urban stray light effects on free-space QKD

2.1. The power and average photons of stray light

In the Earth's atmospheric environment, various light sources introduce stray light; we can categorize stray light into several sources:[8] background radiation from sunlight, reflected light from the moon, starlight from the sky, zodiacal light from the galaxy, airglow and diffuse reflection, surface reflections from the emission end, channel crosstalk, and artificial lighting from human activities. For urban environments, stray light primarily originates from various light sources associated with human activities. Therefore, in this section, we primarily focus on the impact of artificial lighting in cities on free-space QKD.

In urban environments, the noise introduced by stray light can be described by the N_{stray}, which represents the number of stray photons per pulse at the receiver end. The magnitude of N_{stray} is directly related to the brightness conditions of the atmosphere and other parameters[9] at the receiver end, such as the aperture size of the telescope, the field of view (FOV), and the bandwidth of the spectral filter at the receiver. Additionally, the power of the stray light received by the receiving telescope can be expressed as[10]

$$P_{\text{b}} = H_{\text{b}} \times \Omega_{\text{fov}} \times A_{\text{rx}} \times B_{\text{filter}}, \tag{1}$$

where H_{b} represents the background brightness of the atmosphere in $\text{W}\cdot\text{m}^{-2}\cdot\text{Sr}^{-1}\cdot\text{nm}^{-1}$, which is typically related to actual weather conditions, Ω_{fov} denotes the solid angle size of the receiver's FOV in rad, A_{rx} is the aperture size of the receiving telescope in m, and B_{filter} represents the bandwidth of spectral filter in nm at the receiving end. Some typical sky brightness levels under different weather conditions are presented in Table 1.

Table 1. Typical sky brightness values in different urban areas and weather conditions.[11]

Conditions	Illuminance (mlux)
Suburban night sky (clear)	2–45
Suburban night sky (overcast)	30–150
Urban night sky (clear)	7–65
Urban night sky (overcast)	30–500

Based on the illumination value of stray light in the urban night sky, different values can be selected, along with specific parameters at the receiving end and other parameter values. Thus, the stray noise received at the receiver can be determined.

We can calculate values of P_{b} through Eq. (1) to derive the number of stray photons per pulse received at the detector:[8]

$$N_{\text{stray}} = \frac{P_{\text{b}} \cdot \lambda_{\text{N}}}{h \cdot c} \tag{2}$$

where h is the Planck constant, λ_{N} is the central wavelength of stray light, and c is the speed of light.

2.2. Satellite-ground link and QBER estimation model

A satellite-ground QKD link involves transmitting quantum states, typically encoded in photons, from a satellite to a ground station. This transmission must travel through the Earth's atmosphere, which introduces various challenges, such as absorption, scattering, and turbulence. In this section, we will provide an introduction to the satellite-to-ground down-link scenario and QBER estimation model that accounts for stray light.

Figure 1 illustrates the down-link scenario. On the transmitter side, a laser beam is transmitted through the atmosphere and arrives at the receiver. Meanwhile, the artificial light from urban area interacts with the atmosphere through scattering and reflection, thus the telescope receives stray light and signal light at the same time.

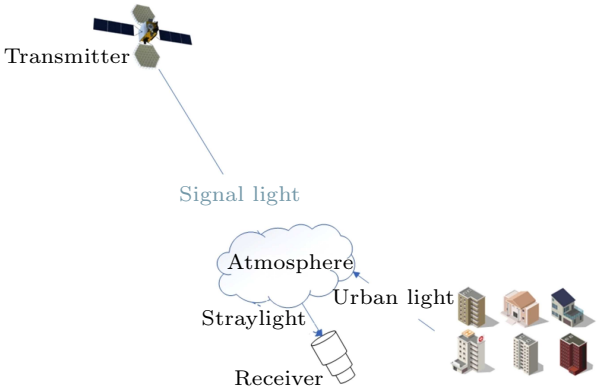


Fig. 1. Satellite–ground link.

In this work, we use QBER to describe the influence of urban stray light. Based on the definition of QBER, it can be expressed as follows:[12]

$$\text{QBER} = \frac{N_{\text{wrong}}}{N_{\text{wrong}} + N_{\text{right}}} = \frac{R_{\text{wrong}}}{R_{\text{wrong}} + R_{\text{right}}}, \tag{3}$$

where N_{wrong} and N_{right} are the number of wrong bits and right bits, respectively. Also, we can use the rate (R) to describe QBER. When the QBER exceeds 11%,[25] the quantum channel is typically considered to be compromised and unable to generate secure keys.

When considering the various noises introduced from external sources, N_{wrong} in Eq. (3) can be expressed as

$$N_{\text{wrong}} = N_{\text{dc}} + N_{\text{stray}} + N_{\text{SOP}} + N_{\text{AP}}, \tag{4}$$

where N_{dc} is the dark count rate, N_{SOP} is polarization errors when utilizing polarization encoding, and N_{AP} is after-pulsing. In this work, we considered the polarization-encoded decoy-state BB84 protocol with weak and vacuum states due to its high key rates, longer effective transmission distance, and enhanced resistance to attacks. Therefore, a more generic QBER expression can be represented as[13]

$$E_{\mu} = \frac{e_0 Y_0 + e_{\text{pol}} \times (1 - \text{e}^{-(t_{\text{link}} \times \mu \times s)})}{Q_{\mu}}, \tag{5}$$

where $Q_\mu = Y_0 + (\mathrm{e}^{-(t_{\mathrm{link}}\times\mu\times s)})$ is the gain of signal states. μ is the average photon number of signal states, and e_0 is the error rate of random background noise and has different values for different protocols. Here, $e_0 = 0.5$ for BB84. $1-\mathrm{e}^{-(t_{\mathrm{link}}\times\mu\times s)}$ is the detection probability of incoming signal state photons. In this expression, we should notice a critical parameter s, which represents the ratio of signal pulses to decoy and vacuum pulses at the transmitter. e_{pol} is the probability of an incorrect bit at the receiver due to polarization errors and can be calculated using the following expression:[14]

$$e_{\mathrm{pol}} = \frac{1}{ER+1} + \frac{ER-1}{ER+1}\sin^2(\theta), \tag{6}$$

where θ is the basis deviation and ER corresponds to the polarization extinction ratio. In the expression of Q_μ, Y_0 is the background detection probability, which can be expressed as[15]

$$Y_0 = 4d\times\Delta t + N_{\mathrm{stray}}\times\eta_{\mathrm{op}}\times\eta_{\mathrm{qrx}}. \tag{7}$$

The noise due to dark counts of a single photon detector depends on the dark count rate d and the detector's gating window Δt. N_{stray} is the number of stray photons mentioned in previous text. η_{op} corresponds to receiver front end optics throughput, η_{qrx} is the quantum receiver efficiency, encompassing the process from free-space to fiber coupling which is related to specific chain architecture. The total efficiency of entire transmission link t_{link} is expressed as

$$t_{\mathrm{link}} = \eta_{\mathrm{geo}}\times\eta_{\mathrm{atm}}\times\eta_{\mathrm{point}}\times\eta_{\mathrm{qrx}}\times\eta_{\mathrm{op}}, \tag{8}$$

where η_{geo} is the geometric loss factor related to the specific configuration of the link, expressing as[16]

$$\eta_{\mathrm{geo}} = \left(\frac{D_{\mathrm{rx}}}{D_{\mathrm{tx}}+Div\times R}\right)^2, \tag{9}$$

where D_{tx} and D_{rx} are the aperture diameters of transmitter and receiver, respectively, R represents the distance between ground station and satellite, Div is the divergence estimation of transmitter telescope. η_{atm} is the atmospheric loss factor and calculated from actual atmosphere environment. η_{point} corresponds to loss factor due to beam pointing errors.

In a SPAD detector, trapped carriers trigger an avalanche, leading to the generation of non-photon detection pulses, causing false counts and an increase in the QBER. We can use after-pulsing probability P_{AP} to describe this phenomenon. Thus, Eq. (5) can be modified as follows:[17]

$$E_\mu = \frac{e_0 Y_0' + (e_{\mathrm{pol}} + e_0 P_{\mathrm{AP}})(1-\mathrm{e}^{-(t_{\mathrm{link}}\cdot\mu\cdot s)})}{Y_0' + (1-\mathrm{e}^{-(t_{\mathrm{link}}\cdot\mu\cdot s)})(1+P_{\mathrm{AP}})}, \tag{10}$$

where P_{AP} is after-pulsing probability, $Y_0' = Y_0(1+P_{\mathrm{AP}})$ corresponds to error counts due to the detector's after-pulsing.

For a SNSPD detector, due to the absence of after-pulsing, Eq. (4) is modified to $N_{\mathrm{stray}} = N_{\mathrm{dc}} + N_{\mathrm{stray}} + N_{\mathrm{SOP}}$ and the QBER should be expressed as follows:

$$E_\mu = \frac{e_0 Y_0 + e_{\mathrm{pol}}(1-\mathrm{e}^{-(t_{\mathrm{link}}\cdot\mu\cdot s)})}{Y_0 + (1-\mathrm{e}^{-(t_{\mathrm{link}}\cdot\mu\cdot s)})}. \tag{11}$$

Combining Eq. (1), (2) and (7), the QBER can be finally written as follows:

$$E_\mu = \frac{e_0 Y_0 + e_{\mathrm{pol}}(1-\mathrm{e}^{-(t_{\mathrm{link}}\cdot\mu\cdot s)})}{4d\times\Delta t + \frac{H_{\mathrm{b}}\cdot\Omega_{\mathrm{fov}}\cdot A_{\mathrm{rx}}\cdot B_{\mathrm{filter}}}{h\cdot c}\cdot\eta_{\mathrm{op}}\cdot\eta_{\mathrm{qrx}} + (1-\mathrm{e}^{-(t_{\mathrm{link}}\cdot\mu\cdot s)})}. \tag{12}$$

Since increasing both the FOV and aperture diameter of the receiving telescope enhances light collection efficiency, we hypothesize that this configuration may mitigate stray light effects on the QBER. Such reduction could potentially suppress the QBER below the 11% threshold during key distribution, thereby ensuring valid key generation between communicating parties.

2.3. Parameter setting and simulation results

In this work, some key parameters for the simulation are shown in Table 2.[32]

Table 2. Parameters setting.

Symbol	Parameter	Value
λ	wavelength	1550 nm
λ_{N}	stray light central wavelength	600 nm
e_0	error rate	0.5
μ	mean photon of signal state	0.5
e_{pol}	polarization error	1%
d_{SNSPD}	dark count rate	5 Hz
Δt	gating window[18]	1 ns
η_{op}	optics throughput	75%
η_{qrx}	receiver efficiency	50%
η_{point}	pointing error loss	3 dB
η_{atm}	atmospheric loss[19]	4 dB
D_{tx}	transmitter aperture	0.2 m
D_{rx}	receiver aperture	1.2 m
R	slant range	900 km
B_{filter}	spectral filter bandwidth	0.1 nm
P_{AP}	after-pulsing probability	0%

According to Eq. (13), the relationship between QBER and FOV is represented in Fig. 2. As shown in Fig. 2, the QBER increases with the FOV of the receiving telescope under different levels of urban light. Furthermore, the QBER under cloudy conditions is higher than that under clear skies, indicating that the interaction between stray light and cloud layers induces stronger scattering and reflection, leading to the reception of more stray photons at the ground station. When the FOV range reaches 100 μrad, the QBER values under all conditions exceed the 11% threshold, rendering the channel vulnerable to eavesdropping and incapable of secure key generation.

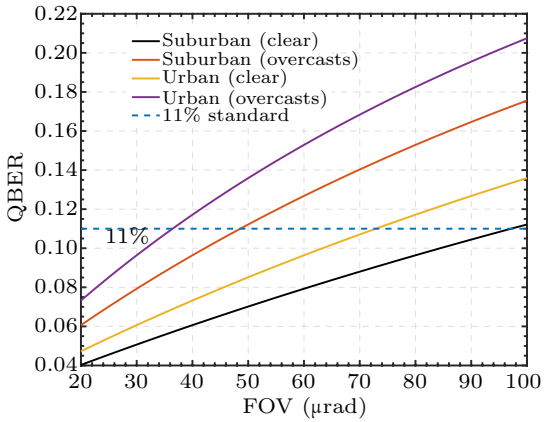


Fig. 2. The relationship between QBER and FOV of a receiver with $D_r = 1.2$ m in different urban areas under different weather conditions.

Figure 3(a) illustrates the variation of QBER with respect to the receiver aperture diameter. As shown, when FOV is identical, the QBER gradually decreases with increasing receiver diameter, indicating that a larger aperture can mitigate the impact of stray light. When the diameter exceeds 0.85 m, the QBER is below 11% under all situations. However, as shown in Fig. 3(b), increasing the diameter also leads to a higher number of stray photons entering the receiver. When the diameter exceeds 0.8 m, the number of stray photons rises rapidly. Beyond this point, the QBER no longer decreases rapidly and instead nearly stabilizes.

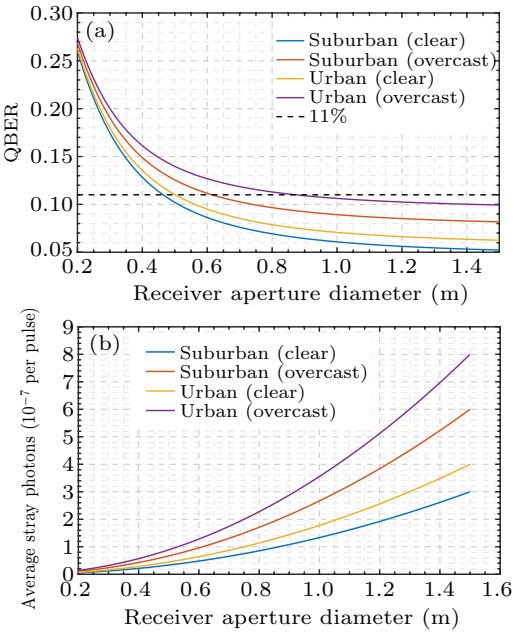


Fig. 3. FOV = 30 μrad, (a) QBER as a function of diameter of receiver aperture in urban and suburban areas under different weather conditions. (b) Variation of average stray photons per pulse with receiver diameter.

In summary, in order to mitigate the impact of stray light on QBER in the urban atmosphere, we can decrease the receiver's FOV and increase the aperture diameter simultaneously. For different values of FOV, we can find a critical diameter beyond which the QBER remains below the 11% threshold, enabling secure key generation.

3. Impacts of urban aerosol particles on free-space QKD

Aerosol particles primarily cause scattering and extinction effects on optical transmission in free space. Depending on the relationship between particle size and light wavelength, we can divide scattering types into Rayleigh and Mie. Rayleigh scattering occurs when the particle size is much smaller than the incident wavelength, while Mie scattering dominates when the particle size is comparable to the wavelength. The composition of atmospheric aerosol particles varies significantly across urban locations, depending on geographical position. For systematic analysis, we categorize cities into coastal (the distance to the sea is usually less than 50 km) and inland types (the distance to the sea is generally greater than 200 km). Coastal urban atmospheres are predominantly characterized by marine aerosols, notably sea salt particles.[31] In contrast, inland urban areas typically contain anthropogenic aerosols, such as combustion-generated soot and insoluble particles.

3.1. The size distribution characteristics of the aerosol particles

The size and shape distribution of aerosol particles exhibit significant complexity, with distinct particle morphologies demonstrating different properties and resulting in varying impacts. To facilitate modeling and analysis, aerosol particles are commonly approximated as homogeneous spheres, where the particle size is represented by the radius of the spherical equivalent. Therefore, the size parameter of aerosol particles can be characterized by[20]

$$x = \frac{2\pi r}{\lambda}, \tag{13}$$

where r is the radius of particles in μm and λ is the light wavelength. The type of scattering depends on the range of x: Rayleigh scattering dominates when $x < 0.1$, while Mie scattering prevails for $0.1 \leq x < 50$.

The size distribution of aerosol particles in a medium follows specific statistical characteristics and can be described using various distribution functions. Currently, the log-normal distribution function is widely employed, which can be expressed as[21]

$$n(r) = \frac{\mathrm{d}N}{\mathrm{d}R} = \frac{N_0}{\sqrt{2\pi}\cdot r\cdot \sigma_{\mathrm{gm}}} \cdot \exp\left(-\frac{(\ln r - \ln r_{\mathrm{gm}})^2}{2\ln^2 \sigma_{\mathrm{gm}}}\right), \tag{14}$$

where N_0 is the number density of aerosol particles, r_{gm} and σ_{gm} denote the average radius of particles in μm and the standard deviation, respectively. The size distribution of various aerosol particles is described once r_{gm} and σ_{gm} are specified.

Another common size distribution function is known as the Junge distribution, which can be expressed as[21]

$$n(r) = N_0 \frac{\alpha r_1^{\alpha} r_2^{\alpha}}{r_2^{\alpha} - r_1^{\alpha}} r^{-\alpha}, \tag{15}$$

where α is generally between 2 and 3, and r_1 and r_2 are distribution boundaries of radius r. In this study, we adopt the log-normal distribution to characterize the size distribution of aerosol particles.

Table 3. Values of r_{gm} and σ_{gm} in different Rh.[22]

Component	r_{gm} (50%)	r_{gm} (70%)	r_{gm} (80%)	r_{gm} (95%)	σ_{gm}
Insoluble	0.471	0.471	0.471	0.471	2.512
Sea salt	2.82	3.17	3.49	5.11	2.03
Soot	0.0118	0.0118	0.0118	0.0118	2.00

The relationship between relative humidity (Rh) and the parameters r_{gm}, σ_{gm} for three typical urban aerosol particles is presented in Table 3.

As shown in Table 3, r_{gm} of sea salt particles increases with rising Rh, whereas soot and insoluble aerosol particles show no significant dependence of r_{gm} on humidity variation.

For $N_0 = 10^6$ m^{-3}, Fig. 4 illustrates the size distribution of different aerosol particles. Figure 4(a) displays the size distribution of sea salt particles under different Rh conditions. As humidity increases, a greater abundance of larger-radius particles is observed. Figure 4(b) presents the size distribution of insoluble particles, which are primarily confined within a 1 μm radius. Figure 4(c) illustrates the size distribution of soot particles, demonstrating significantly smaller radii compared to both sea salt and insoluble particles, with a more concentrated distribution pattern.

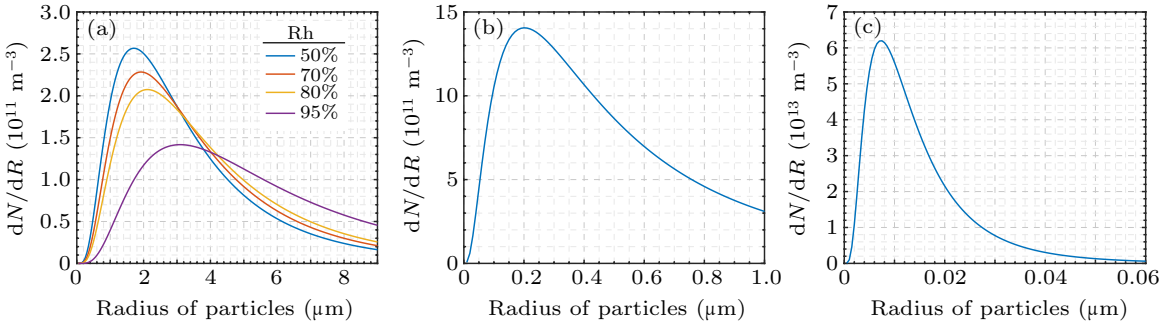


Fig. 4. (a) The sea salt size distribution under different Rh. (b) Insoluble particles distribution. (c) Soot aerosol size distribution.

3.2. Aerosol extinction effects

When the light propagates through aerosol particles, both absorption and scattering effects occur, leading to intensity attenuation. This phenomenon critically impacts free-space QKD performance. Consequently, comprehensive investigation of extinction characteristics across different aerosol types becomes essential for practical QKD implementation in urban environments. The extinction coefficient serves as a quantitative measure of the strength of extinction effects, which can be expressed as

$$k_{ext} = \pi \int_{r_1}^{r_2} Q_{ext} \cdot n(r) \cdot r^2 \, dr, \tag{16}$$

where r_1 and r_2 are lower and upper bounds of aerosol particle radius, respectively, $n(r)$ denotes the size distribution function introduced in the preceding section. Q_{ext} is the extinction efficiency factor and is given as[23]

$$Q_{ext} = \frac{2}{x^2} \sum_{n=1}^{\infty} (2n+1) \mathrm{Re}(a_n + b_n), \tag{17}$$

where Re denotes the real part of a complex quantity, we mainly take Mie scattering into consideration and a_n, b_n represent Mie coefficients:[20]

$$a_n = \frac{\psi_n'(mx)\psi_n(x) - m\psi_n(mx)\psi_n'(x)}{\psi_n'(mx)\xi_n(x) - m\psi_n(mx)\xi_n'(x)}, \tag{18}$$

$$b_n = \frac{m\psi_n'(mx)\psi_n(x) - \psi_n(mx)\psi_n'(x)}{m\psi_n'(mx)\xi_n(x) - \psi_n(mx)\xi_n'(x)}, \tag{19}$$

where $\psi_n(x)$ and $\xi_n(x)$ are Ricatti-Bessel functions, which are defined as

$$\psi_n(x) = \sqrt{\frac{\pi x}{2}} J_{n+\frac{1}{2}}(x), \tag{20}$$

$$\xi_n(x) = \sqrt{\frac{\pi x}{2}} H_{n+\frac{1}{2}}(x), \tag{21}$$

where $\psi_n'(x)$ and $\xi_n'(x)$ are the first derivatives , and m is the refractive index of particles. Under Mie scattering conditions, the value of n exhibits dependence on the particle size parameter x, having a maximum that can be calculated as follows:[24]

$$n_{max} = x + 4x^{\frac{1}{3}} + 2. \tag{22}$$

The complex refractive indexes of common urban aerosol particles under different humidities are presented in Table 4.

Based on Eqs. (16) and (17), the variation of the extinction coefficient with radius for sea salt aerosols under different humidity levels is obtained, as illustrated in Fig. 5.

We can find that the extinction coefficient exhibits a gradual rise with sea salt particle radius, enhancing optical attenuation. Concurrently, due to the hygroscopicity of sea salt particles, elevated Rh leads to the production of more particles with larger radii, which augments the extinction coefficient, and this humidity dependence becomes more pronounced for larger particles.

Table 4. Complex refractive indexes[25] of three types particles for $\lambda = 1550$ nm.

Rh	50%	70%	80%	95%
Sea salt	$1.354 - 2.884 \times 10^{-4}$i	$1.344 - 2.622 \times 10^{-4}$i	$1.339 - 2.466 \times 10^{-4}$i	$1.327 - 2.149 \times 10^{-4}$i
Soot	$1.77 - 0.46$i	$1.77 - 0.46$i	$1.77 - 0.46$i	$1.77 - 0.46$i
Insoluble	$1.41 - 0.008$i	$1.41 - 0.008$i	$1.41 - 0.008$i	$1.41 - 0.008$i

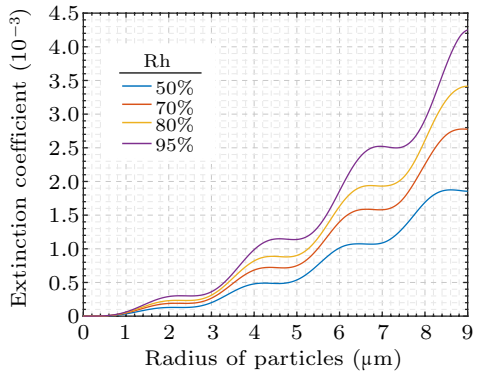


Fig. 5. The extinction coefficient variation of sea salt with particle radius under different humidities. $\lambda = 1550$ nm, $N_0 = 10^6$ m^{-3}.

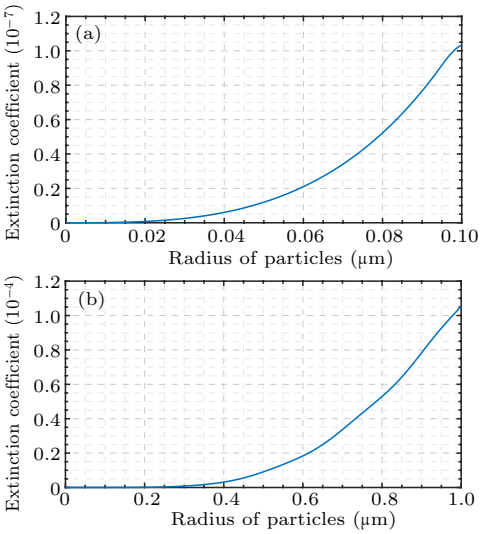


Fig. 6. (a) The extinction coefficient variation of soot particles ($m = 1.77 - 0.46$i) with radius. (b) Variation of the extinction coefficient of the insoluble particles with radius ($m = 1.41 - 0.008$i).

Simultaneously, the relationship between the extinction coefficient and particle radius can be derived for soot and insoluble aerosol particles. As shown in Figs. 6(a) and 6(b), the extinction coefficients of both aerosol types increase with particle radius and exhibit an exponential rise in extinction coefficient with radius. Soot aerosols maintain lower values compared to insoluble particles across all size ranges. Compared to sea salt, both soot and insoluble aerosols exhibit lower extinction coefficients, indicating weaker light extinction effects.

3.3. The effects of aerosol particles on atmosphere transmittance

Due to extinction effects, the atmospheric transmittance in urban environments is influenced by aerosol particles and can be expressed as follows:

$$T = \mathrm{e}^{-k_{\mathrm{ext}} \cdot s} = \exp\left(-\pi \int_{r_1}^{r_2} Q_{\mathrm{ext}} \cdot n(r) \cdot r^2 \,\mathrm{d}r \cdot s \right), \quad (23)$$

where s denotes the straight-line distance between the transmitter and the receiver.

Figure 7 depicts the variation of atmospheric transmittance with particle radius for sea salt and insoluble aerosol particles.

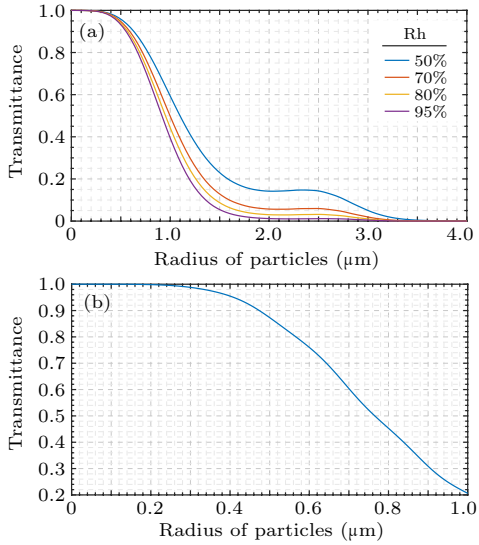


Fig. 7. (a) Transmittance variation with sea salt particle radius under different humidities. (b) The variation of transmittance with insoluble aerosol particles.

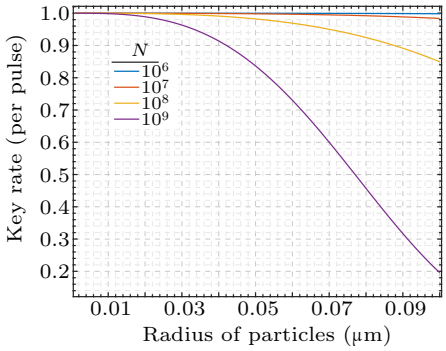


Fig. 8. The impacts of particle radius and number density on transmittance with soot aerosol.

For both sea salt and insoluble aerosols, increasing particle radius reduces atmospheric transmittance. In Fig. 7(a), elevated Rh enhances the transmittance reduction by sea salt particles and transmittance decreases with rising humidity at a constant particle radius.

The transmittance variation with soot particle radius under different particle number densitise is shown in Fig. 8.

As demonstrated in Figs. 5 and 6(a), soot aerosols exhibit the weakest extinction effects among the three particle types. Consequently, under the same number density and transmission distance, soot aerosols impose the minimal impact on atmospheric transmittance. The transmittance decline becomes

progressively more pronounced with increasing N, showing a marked reduction when $N = 10^9$ m^{-3}, corresponding to moderate haze[30] mainly caused by traffic emissions and combustion.

4. Key rate analysis

In this section, we analyze the impact of inland urban areas and coastal city aerosols on the practical key rate of QKD protocols. To achieve longer transmission distance and higher key rates, we employ the polarization-encoded decoy state BB84 protocol with weak and vacuum states proposed by Wang and Lo[26–28] in 2005. The key rate can be expressed as[29]

$$R = q\{-Q_\mu f(E_\mu) H_2(E_\mu) + Q_1^{L,v,0}[1 - H_2(e_1^{U,v,0})]\}, \quad (24)$$

where $H(x)$ is the binary Shannon information function, different protocols have different q values, for BB84, $q = 1/2$. $f(x)$ is the bidirectional error correction efficiency, $Q_1^{L,v,0}$ is the lower-bound of single photon gain and can be represented as follows:[28]

$$Q_1^{L,v,0} = \frac{\mu^2 \mathrm{e}^{-\mu}}{\mu v - v^2}\left(Q_v \mathrm{e}^{v} - Q_\mu \mathrm{e}^{\mu}\frac{v^2}{\mu^2} - \frac{\mu^2 - v^2}{\mu^2} Y_0\right), \quad (25)$$

where Y_0 is the dark count rate, Q_μ and Q_v are the gain of signal state μ and decoy state v, respectively, which have the form

$$Q_\mu = \sum_{i=1}^{\infty} Y_i \frac{\mu^i}{i!}\mathrm{e}^{-\mu} = Y_0 + 1 - \mathrm{e}^{-\eta\mu}, \quad (26)$$

$$Q_v = \sum_{i=1}^{\infty} Y_i \frac{v^i}{i!}\mathrm{e}^{-v} = Y_0 + 1 - \mathrm{e}^{-\eta v}. \quad (27)$$

Here, η represents the total transmittance of the channel that contains these components: the receiver's transmittance $\eta_\mathrm{B} = t_\mathrm{Bob}\eta_\mathrm{D}$, where t_Bob is the transmittance of internal optical path in the detector, and η_D is the detector efficiency. According to Eq. (23), the transmittance can be described as $T_\mathrm{total} = \exp(-\pi \int_{r_1}^{r_2} Q_\mathrm{ext} \cdot n(r) \cdot r^2 \mathrm{d}r \cdot s) \cdot t_\mathrm{Bob} \cdot \eta_\mathrm{D}$, and $e_1^{U,v,0}$ is the upper-bound of single photon bit error rate which can be expressed as[29]

$$e_1^{U,v,0} = \frac{E_v Q_V \mathrm{e}^{v} - e_0 Y_0}{Y_1^{L,v,0} v}, \quad (28)$$

where $Y_1^{L,v,0} = \frac{\mu}{\mu v - v^2}\left(Q_v \mathrm{e}^{v} - Q_\mu \mathrm{e}^{\mu}\frac{v^2}{\mu^2} - \frac{\mu^2 - v^2}{\mu^2} Y_0\right)$. For the BB84 protocol, q is set to 0.5.

Figure 9 illustrates the dependence of key rate on the radii of sea salt and insoluble aerosol particles in urban environments. Increasing particle radii for both aerosol types leads to reduced key rate. In Fig. 9(a), a significant decrease in key rate occurs when particle radii exceed 2.5 μm. At a fixed particle radius, the key rate decreases with rising Rh, with more pronounced degradation at higher Rh levels. Notably, elevated humidity levels accelerate the decline in key rates. In Fig. 9(b), when $r > 0.4$ μm, the key rate decreases significantly, compared to sea salt particles, insoluble aerosols exhibit weaker impacts on the key rate.

Figure 10 shows the relationship between key rate and soot particle radius under different N values and transmission distances.

As shown in Fig. 10(a), under identical transmission distances and number densities ($s = 15$ km, $N = 10^6$ m^{-3}), soot aerosols exhibit the weakest impact on the key rate compared to sea salt and insoluble particles. When $N = 10^9$ m^{-3} (moderate haze), the key rate demonstrates significant degradation across all three transmission distances. Notably, the soot-dominated environment enables longer achievable transmission distances under equivalent conditions.

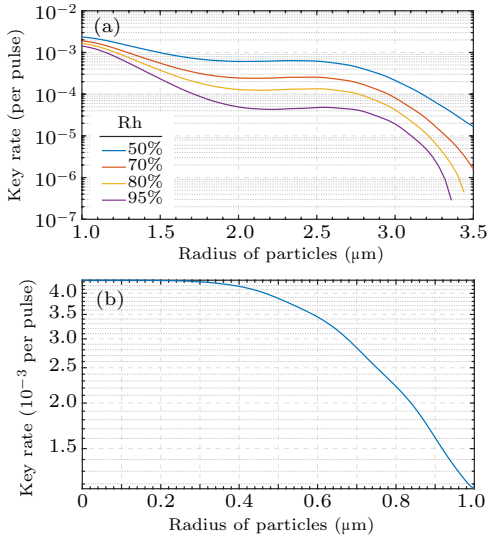


Fig. 9. (a) The variation of key rate with sea salt particle radius under different Rh values. (b) Relationship between key rate and insoluble particle radius ($s = 15$ km).

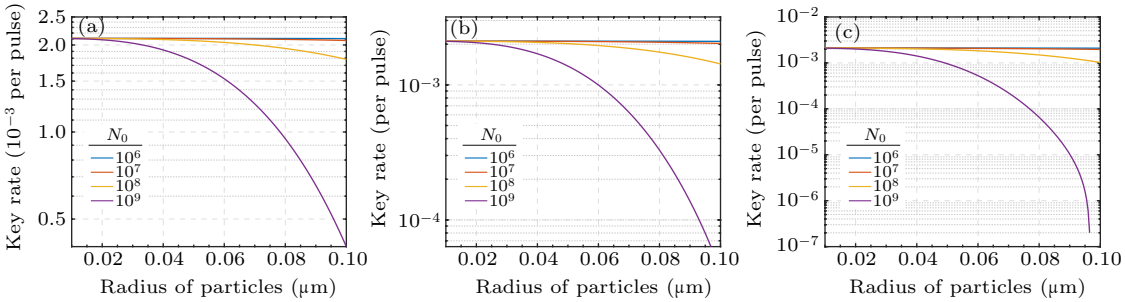


Fig. 10. (a) The variation of key rate with soot particle radius under different particle number density, ($s = 15$ km) Relationship between key rate and soot particle radius at (b) $s = 35$ km and (c) $s = 65$ km.

5. Conclusion

In this paper, based on the satellite to ground scenario, we first discussed the impacts of stray light on QBER under different urban zones and varying weather conditions. The results show that as FOV of the telescope increases, the QBER exhibits an upward trend across different urban regions and varying weather conditions. Under identical weather conditions, QBER values in suburban areas are significantly lower than those in urban areas. Moreover, within the same urban region, QBER is substantially higher on overcast nights compared to clear night, which indicated that the interaction between stray light and cloud layers induces stronger scattering and reflection. When the FOV of the telescope remains constant, increasing diameter leads the QBER to decrease. The above analysis demonstrates that employing a telescope with smaller FOV and larger diameter at the receiving end can effectively mitigate the impact of urban stray light on QKD and for different FOV, a critical diameter value can be found beyond which the QBER remains below the 11% threshold and ensures that a secure secret key is generated.

Second, we systematically discussed the impact of urban atmospheric aerosols by analyzing three types of aerosol particle: sea salt particles in a coastal city, and soot and insoluble particles in an inland city. According to the log-normal distribution model and Mie scattering, we calculated the extinction coefficient of three particle types. The results indicate that both soot and insoluble aerosols show weaker light extinction effects compared to sea salt. The size distribution and refractive index of sea salt are all affected by humidity: elevated Rh leads to higher extinction coefficient and this humidity-dependence becomes more pronounced for larger particles radius. The key rate analysis was carried out in Section 4, finding that in coastal cities, with $N = 10^6$ m^{-3} and $s = 15$ km, there is a significant decrease in key rate when the radius exceeds 2.5 μm in a sea salt-dominated atmosphere. Sea salt shows the greatest impacts compared to soot and insoluble particles. Under the same conditions, in inland cities we can obtain a higher key rate than that in coastal cities and soot aerosols exhibit a weaker impact compared to insoluble particles. When increasing the number density to 10^9 m^{-3}, corresponding to moderate haze weather, the soot-dominated environment enables longer achievable transmission distances to 65 km. Our work may provide a certain reference for performing satellite to ground free-space QKD in urban area during night time and offer a reference framework for developing urban quantum internet systems in actual environments.

References

[1] Yang X L, Li Y Q and Li H W 2025 *Chin. Phys. B* 34 020301
[2] Bennett C H, Brassard G, *et al*. 1984 *IEEE International Conference on Computers, Systems and Signal Processing*
[3] Alessia S, Giulio F, Francesco P, *et al*. 2022 *Quantum Science and Technology* **7** 045029
[4] Ricklin J, Hammel S, Easton F, *et al*. 2006 *Optic. Fiber. Common. Rep* **3** 10297
[5] Wang F Z, Du W H, Yuan Q, *et al*. 2021 *Atmosphere* **12** 121608
[6] Tomasz S 2021 *Remote Sensing* **13** 1654
[7] Vasylyev D, Semenov A A and Vogel W 2016 *Phys. Rev. Lett.* **117** 090501
[8] Stefanie H, Davide O, Leonard V, *et al*. 2024 *Optical Engineering* **63** 041211
[9] Lu Y, Xu X P, Zhang N, *et al*. 2024 *IEEE Access* **12** 33948
[10] Mark T G, Michael B F, Brett A S, *et al*. 2015 *Opt. Express* **23** 23924
[11] Andreas H, Thomas P, Salvador J, *et al*. 2018 *Journal of Quantitative Spectroscopy and Radiative Transfer* **205** 278
[12] Schranz A and Udvary E 2019 *Optics and Laser Technology* 181
[13] Nelson J M, Ferreira F S, Armando N P, *et al*. 2010 *Journal of Lightwave Technology* **29** 209643
[14] Wu J C, Zhang L, Jia J J, *et al*. 2016 *Opt. Express* **28** 10746
[15] Khanna A, Majumder S, Adarsh J, *et al*. 2024 *IET Quantum Communication* **5** 12081
[16] Tahir M, Sultan M Y, Muhammad S K *et al*. 2018 *Acta Phys. Polonica A* **134** 275
[17] Papapanos C, Zavitsanos D, Raptakis A, *et al*. 2020 arXiv preprint arXiv:2010.03358
[18] Argiris N, Nikolaos K L, Aristeidis S, *et al*. 2024*IEEE Aerospace and Electronic Systems Magazine* **39** 23
[19] Liao S K, *et al*. 2017 *Nat. Photon.* **11** 509
[20] Wolf S and Voshchinnikov N V 2004 *Computer Physics Communications* **162** 114
[21] Olivier B 2009 *Atmospheric Aerosols Properties and Climate Impacts* (Berlin: Springer)
[22] Jorg A 1997 *American Meteorological Society* **15** 1043
[23] Du H 2004 *Appl. Opt.* **43** 1951
[24] Bohren C F and Huffman D R 2008 *Absorption and Scattering of Light by Small Particles* (Germany: John Wiley)
[25] Hess M, Koepke P and Schult I 1998 *Bulletin of the American Meteorological Society* **79** 5
[26] Wang X B 2005 *Phys. Rev. Lett.* **94** 230503
[27] Lo H K, Ma X and Chen K 2005 *Phys. Rev. Lett.* **94** 230504
[28] Wang X B 2005 *Phys. Rev. A* **72** 012322
[29] Ma X, Qi B, Zhao Y, *et al*. 2005 *Phys. Rev. A* **72** 012326
[30] Titos G, Lyamani H, Querol X, *et al*. 2012 *Journal of Geophysical Research: Atmospheres* **117** D4
[31] Rajae M, Mohammed D and Abdelmoula B 2020 *Air Qual Atmos Health* **13** 25
[32] Ntanos A, Nikolaos K L, *et al*. 2024 *IEEE Aerospace and Electronic Systems Magazine* **39** 16